Tunable p-Type Conductivity and Transport Properties of AlN Nanowires *via* Mg Doping

Yong-Bing Tang,[†] Xiang-Hui Bo,[†] Jun Xu,[†] Yu-Lin Cao,[†] Zhen-Hua Chen,[†] Hai-Sheng Song,[†] Chao-Ping Liu,[†] Tak-Fu Hung,[†] Wen-Jun Zhang,[†] Hui-Ming Cheng,[‡,*] Igor Bello,[†] Shuit-Tong Lee,[†] and Chun-Sing Lee[†,*]

[†]Center of Super-Diamond and Advanced Films (COSDAF) and Department of Physics and Materials Science, City University of Hong Kong, Hong Kong SAR, People's Republic of China, and [‡]Shenyang National Laboratory for Materials Science, Institute of Metal Research, Chinese Academy of Sciences, Shenyang 110016, People's Republic of China

ABSTRACT Arrays of well-aligned AlN nanowires (NWs) with tunable p-type conductivity were synthesized on Si(111) substrates using bis(cyclopentadienyl)magnesium (Cp_2Mg) vapor as a doping source by chemical vapor deposition. The Mg-doped AlN NWs are single-crystalline and grow along the [001] direction. Gate-voltage-dependent transport measurements on field-effect transistors constructed from individual NWs revealed the transition from n-type conductivity in the undoped AlN NWs to p-type conductivity in the Mg-doped NWs. By adjusting the doping gas flow rate (0−10 sccm), the conductivity of AlN NWs can be tuned over 7 orders of magnitude from $(3.8-8.5) \times 10^{-6}\ \Omega^{-1}\ \mathrm{cm}^{-1}$ for the undoped sample to $15.6-24.4\ \Omega^{-1}\ \mathrm{cm}^{-1}$ for the Mg-doped AlN NWs. Hole concentration as high as $4.7 \times 10^{19}\ \mathrm{cm}^{-3}$ was achieved for the heaviest doping. In addition, the maximum hole mobility ($\sim$6.4 $\mathrm{cm^2/V\ s}$) in p-type AlN NWs is much higher than that of Mg-doped AlN films ($\sim$1.0 $\mathrm{cm^2/V\ s}$).[2] The realization of p-type AlN NWs with tunable electrical transport properties may open great potential in developing practical nanodevices such as deep-UV light-emitting diodes and photodetectors.

KEYWORDS: aluminum nitride · nanowire arrays · Mg doping · tunable p-type conductivity · field-effect transistors

Aluminum nitride (AlN), as an important group III−V material, has attracted considerable interest due to its unique properties such as a wide and direct band gap (6.2 eV), extremely low electron affinity,[1] and excellent thermal conductivity, rendering AlN a promising candidate for applications in deep-ultraviolet light-emitting diodes (LEDs),[2] field emitters,[3−12] and high-power/high-frequency electronic devices.[13] In addition, AlN has high piezoelectric response and, thus, is a good material for piezoelectric devices.[14,15] However, the devices fabricated from AlN have been limited due to its insulating property and the difficulty of growing highly crystalline AlN.[16] Doping is an efficient approach to tune the electrical properties of semiconductors and has been widely utilized in the semiconductor industry.[17,18] Recently, the success in controlled doping of AlN films has enabled the realization of ultraviolet LEDs with a wavelength of 210 nm, which is the shortest ever reported among semiconductors.[2] As in thin-film devices, the realization of functional devices based on AlN nanostructures depends on the capability of controlling their electrical transport properties, which could be realized *via* appropriate doping.

To date, one-dimensional (1D) AlN nanostructures, such as nanotubes, nanowires, and nanorods, have been synthesized by various routes, such as chloride-assisted growth,[5,10−12,19,20] carbon nanotube-confined reaction,[21,22] arc-discharge,[3,9] direct nitridation of Al powders,[23] and vapor transport method.[6,7,24−26] Additionally, AlN nanostructures doped with different elements such as Fe, Si, Cu, Mn, and Tb have also been prepared, and their corresponding ferromagnetic, field emission, or optical properties were investigated.[25−30] However, there are relatively few studies on the electrical transport properties of undoped or doped 1D AlN nanostructures thus far. Although electrical properties of AlN nanoneedles have been measured to be semiconducting due to unintentional incorporation of Si from the growth substrates,[25] such an AlN nanostructure showed an extremely low conductivity, far below the level required for any practical devices. So far, many issues of doping in AlN nanostructures, such as control of doping type and conductivity, remain unresolved.

Here, we report the realization of tunable p-type conductivity in well-aligned single-crystalline AlN nanowire arrays *via* magnesium doping. Gate-dependent electrical properties of AlN NWs were studied by constructing field-effect transistors (FETs) from single nanowire. It was found that the n-type conductivity of undoped AlN NWs was converted to p-type upon Mg

* Address correspondence to
apcslee@cityu.edu.hk,
cheng@imr.ac.cn.

Received for review December 1, 2010
and accepted April 11, 2011.

10.1021/nn200963k

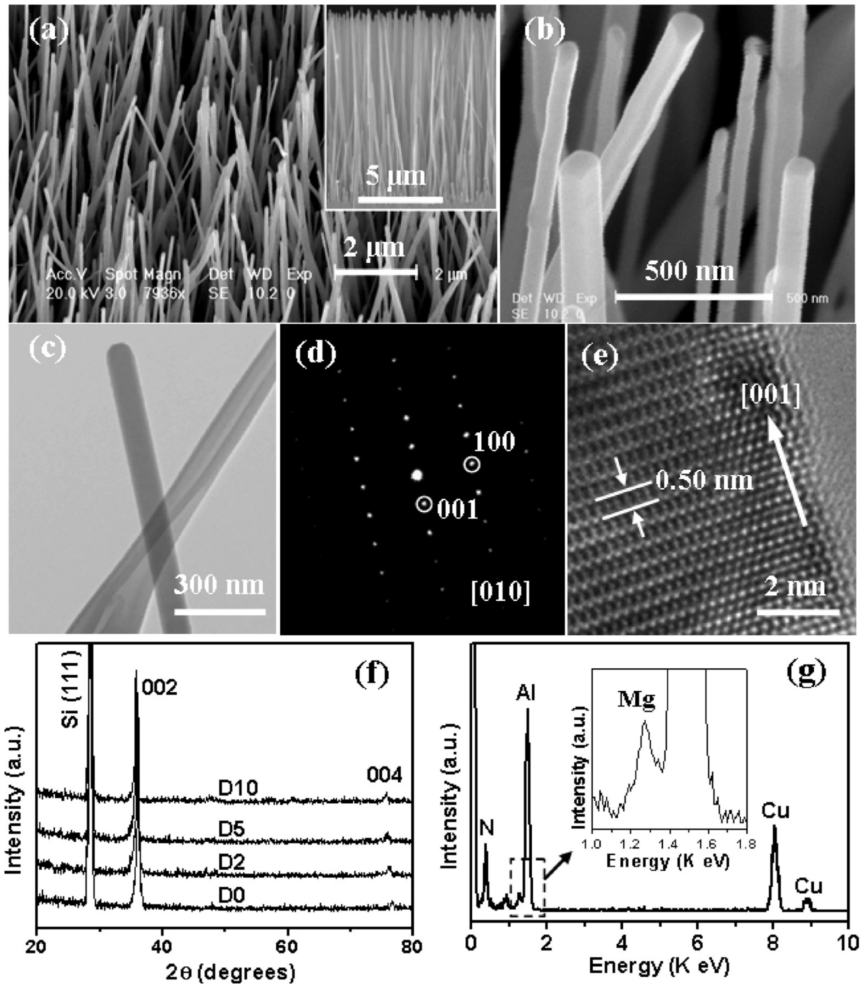

Figure 1. Representative characterizations of Mg-doped AlN NW arrays (sample D10). (a, b) SEM images of Mg-doped AlN NWs. Inset in (a) is a cross-section SEM image. (c) TEM image, (d) corresponding SAED pattern, and (e) HRTEM image of a doped (D10) AlN NW. (f) XRD patterns of each NW sample on Si(111) substrates, including samples D0 (undoped NWs), D2, D5, and D10. (g) EDS spectrum of Mg-doped (D10) AlN NWs. The inset shows the magnified Mg Kα peak.

doping. Furthermore, the conductivity level depends on the dopant concentration and can be tuned over 7 orders of magnitude. The magnesium doping leads to significant improvements in the electrical transport properties of AlN NWs, which should benefit the fabrication of future high-performance AlN nanodevices.

RESULTS AND DISCUSSION

Preparation of Mg-Doped AlN Nanowire Arrays. Undoped and Mg-doped AlN NWs were grown on Si(111) substrates by the chloride chemical vapor deposition (CVD) method. The detailed synthesis process is described in the Experimental Section. $AlCl_3$ and NH_3 were used as Mg and N precursors, respectively. The growth temperature was kept at about 750 °C. Bis-(cyclopentadienyl)magnesium (Cp_2Mg) (99.9%, Aldrich) was evaporated by an independent heater (Figure S1) and subsequently transported by Ar to the growth zone. The flow rate of the doping gas was tuned in the range 0−10 sccm to prepare nanowires with different doping concentrations. Undoped AlN NWs were prepared under the same conditions but with no dopant source.

Characterizations of AlN Nanowire Arrays. In this study, undoped NWs and three doped NW samples prepared with doping gas flow rates of 2, 5, and 10 sccm are denoted as samples D0, D2, D5, and D10, respectively. Figure 1a and b show representative scanning electron microscopy (SEM) images of sample D10. It can be seen that AlN nanowires were relatively uniform on the Si substrate and vertically aligned (Figure 1a, inset). The surfaces of the NWs are smooth and clean without visible impurities. The nanowires have diameters in the range 50−150 nm and lengths about 10 μm. Figure 1c is a typical transmission electron microscopy (TEM) image of the AlN nanowires in sample D10, and the corresponding selected-area electron diffraction (SAED) pattern (Figure 1d) clearly reveals that the nanowire is single-crystalline wurtzite AlN with [001] growth direction (Figure 1e). Structure defects such as stacking faults were rarely observed (Figure S2), suggesting the crystal quality of the AlN NWs is not

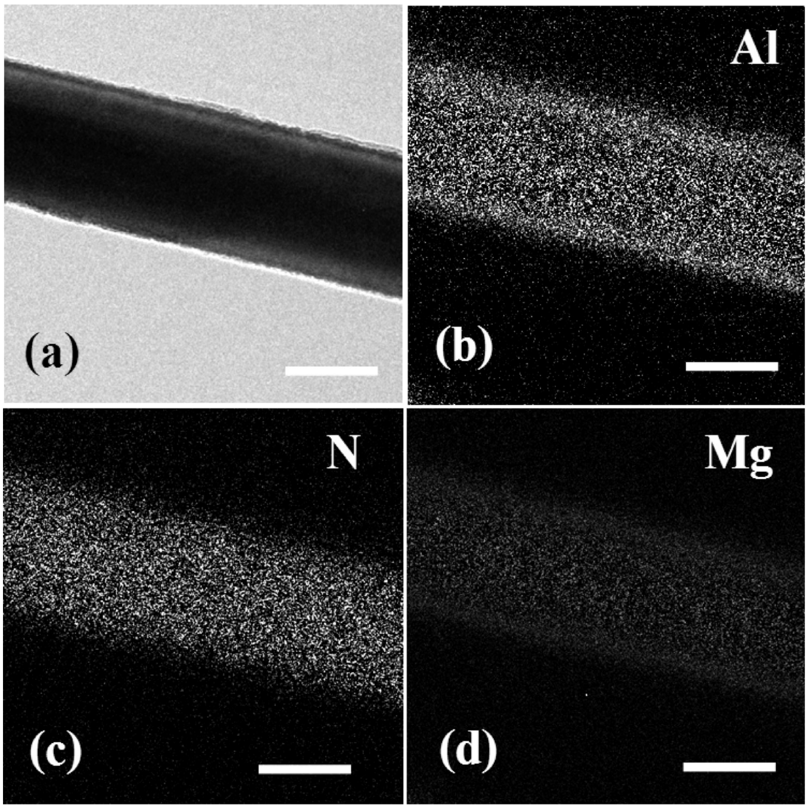

Figure 2. TEM image of a Mg-doped AlN NW in sample D10 (a) and the corresponding Al (b), N (c), and Mg (d) EDS elemental mappings (scale bar: 50 nm).

considerably affected by the Mg incorporation. Morphologies and crystal structures of other samples were found to be similar to those of sample D10.

X-ray diffraction (XRD) patterns of all samples are shown in Figure 1f. Except for the Si(111) peak from substrates, only diffraction peaks from (002) and (004) planes of hexagonal wurtzite AlN were observed. This reveals the epitaxial relationship of AlN(001)//Si(111), as previously reported in epitaxial AlN films grown on Si(111) substrates.[14] Notably, the diffraction peaks from the doped samples slightly shifted to lower angles relative to the undoped sample, indicating lattice parameter broadening along the *c*-axis. This lattice broadening should be attributed to incorporation of Mg into the AlN lattice since Mg^{2+} (0.72 Å) has a larger ionic radius than Al^{3+} (0.535 Å). The wurtzite structure of AlN NWs was further confirmed by XRD analyses measured by detaching the nanowires from the Si substrates (Figure S3).

Energy-dispersive X-ray spectroscopy (EDS) analyses were further performed to evaluate Mg concentration in the doped AlN NWs. For samples D0, D2, and D5, only signals from Al and N could be detected (spectra not shown here) since their Mg content is below the detection limit of EDS (about 0.5 at. %). However, for sample D10 a weak Mg Kα peak at ~1.27 eV (Figure 1g and inset) was detected besides the strong Al and N signals (the Cu signals come from the TEM grid), confirming the existence of Mg. Quantitative analyses on various nanowires in sample D10 reveal that the Mg concentration was 0.6−0.8 at. %. These results were also confirmed by X-ray photoemission spectroscopy (XPS, Figure S4). The trace amount of doped Mg in samples D2 and D5 was probed *via* secondary ion mass spectroscopy (SIMS, Figure S5). The Mg concentrations were estimated to be ~0.13, 0.31, and 0.67 at. %, for doped samples D2, D5, and D10, respectively, while the Mg concentration for the undoped sample is lower than 0.003 at. %, demonstrating Mg was indeed incorporated into AlN nanowires by our doping method. Composition distribution was determined by the EDS elemental mappings, as shown in Figure 2, which reveals Mg element is uniformly distributed in the AlN NW.

Electrical Measurements of Undoped and Mg-Doped AlN Nanowire FETs. To investigate the electrical transport properties of the undoped and Mg-doped AlN NWs, we fabricated AlN NW-based field-effect transistors on SiO_2 (300 nm)/p^+-Si substrates with Ti (100 nm)/Au (50 nm) source−drain electrodes. Gate voltage was applied to the p^+-Si substrate using the standard back-gate geometry.[31,32] To activate Mg dopants, all FETs made of the doped samples were annealed in N_2 at 500 °C for 10 min, as in AlN or GaN thin films.[2,33] The inset in Figure 3a is an SEM image of a typical FET fabricated from a single undoped AlN NW (sample D0)

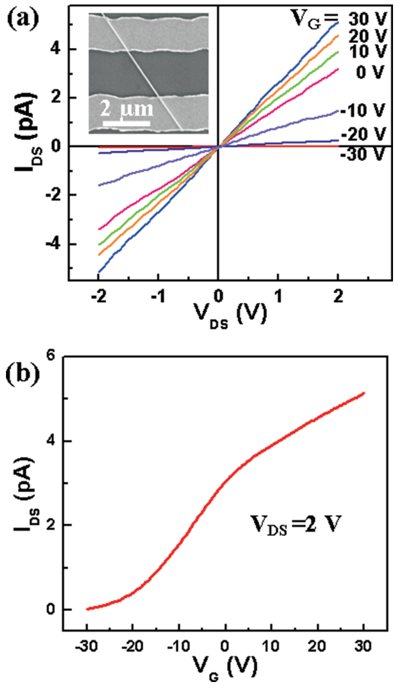

Figure 3. Electrical characteristics of undoped AlN NW FETs (sample D0). (a) $I_{DS}-V_{DS}$ curves of a representative NW FET at different V_G. The inset is an SEM image of the single-NW FET. Diameter of the nanowire is ~90 nm, and effective gate length is about 2.5 μm. (b) $I_{DS}-V_G$ curve plot at V_{DS} = 2 V.

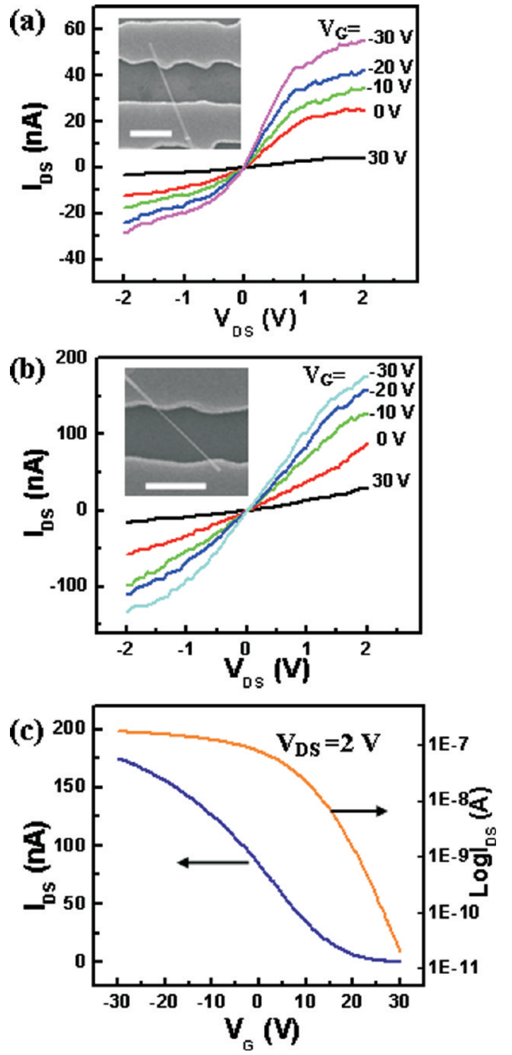

Figure 4. (a) $I_{DS}-V_{DS}$ plots of Mg-doped AlN NWs (sample D2) at different V_G with Ti (100 nm)/Au (50 nm) source–drain electrodes. Inset in (a) is the NW FET (scale bar: 2 μm). (b) $I_{DS}-V_{DS}$ plots of Mg-doped AlN NWs (sample D2) at different V_G with Ni (100 nm)/Au (50 nm) as electrode. Diameter of nanowire is 78 nm, and effective gate length is 2.5 μm. The inset shows a SEM image of the FET (scale bar: 2 μm). (c) Linear and logarithmic plots of $I_{DS}-V_G$ at V_{DS} = 2 V of the FET shown in (b).

with a diameter of ~90 nm. Linear I_{DS} (source–drain current) *vs* V_{DS} (source–drain voltage) curves (Figure 3a) obtained from FETs made of undoped AlN NWs under different gate voltages (V_G varies from -30 to 30 V) indicate a good ohmic contact between the Ti/Au electrodes and the undoped AlN NWs. The conductivity was calculated be about $6.3 \times 10^{-6}\ \Omega^{-1}\ \mathrm{cm}^{-1}$ from the $I_{DS}-V_{DS}$ curve at $V_G = 0$. This value is on the same order of that of AlN nanoneedles ($8 \times 10^{-6}\ \Omega^{-1}\ \mathrm{cm}^{-1}$) grown on Si substrates.[25] However, for a high-purity AlN single crystal, the resistivity is typically in the range $10^{11}-10^{12}\ \Omega$ cm at room temperature. According to the previous report,[25] the observed conductivity in AlN NWs is possibly originated from the Si atoms from Si substrates by thermal diffusion during NW growth. Dependence of I_{DS} on V_G at V_{DS} = 2 V is depicted in Figure 3b, revealing a typical n-type conductivity behavior; that is, the conductance increases with increasing positive V_G. n-Type behavior of the undoped AlN NWs mainly arises from the intrinsic donor defects, such as N vacancies, Al interstitials, and unintentionally doped Si impurity, as previously reported in AlN nanoneedles.[25,28] The electron mobility (μ_e) can be estimated from the channel conductance (g_m) of the FET, $g_m = dI_{DS}/dV_G = \mu C V_{DS}/L^2$ in the linear regime of the $I_{DS}-V_G$ curve, where C is the gate capacitance and L is the effective nanowire length between electrodes. The capacitance is given by $C = 2\pi\varepsilon_0\varepsilon_{SiO2}L/\ln(4h/d)$, where ε_{SiO2} is the dielectric constant of the gate SiO_2 (3.9), h is SiO_2 thickness (300 nm), L is the length of the nanowire channel (2.5 μm), and d is NW diameter (90 nm). Thus C is estimated to be about 2.1×10^{-16} F for this device, and based on this value, the electron mobility was derived to be about $2.3 \times 10^{-5}\ \mathrm{cm}^2/\mathrm{V\ s}$ at V_{DS} = 2 V. Carrier concentration was then calculated from $\rho = 1/\sigma = 1/nq\mu$ to be about $1.7 \times 10^{18}\ \mathrm{cm}^{-3}$.

$I_{DS}-V_{DS}$ curves at different V_G of a typical FET from sample D2 are shown in Figure 4a. The conductivity of the AlN NW changed obviously from n-type to p-type upon Mg doping; that is, the current decreases with increasing positive V_G. On the other hand, the curves are nonlinear and different from those of undoped sample, which is supposed to originate from the work function mismatch between the source–drain electrodes and the Mg-doped AlN NWs. It is expected

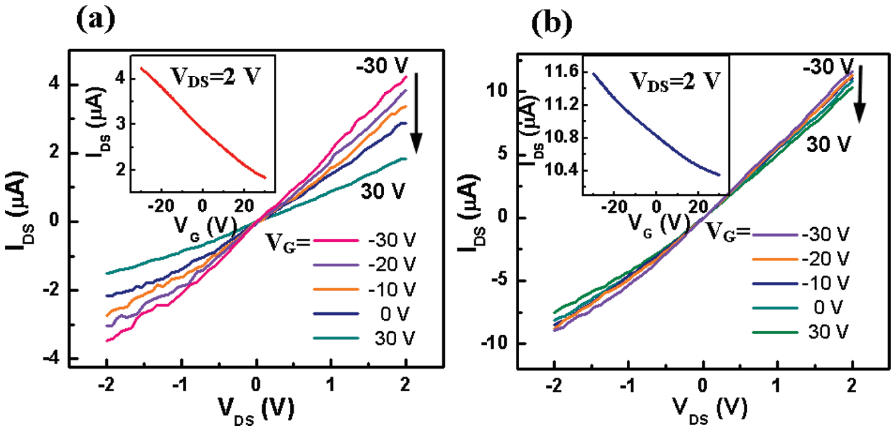

Figure 5. $I_{DS}-V_{DS}$ **plots at different** V_G **of Mg-doped AlN NWs grown with** Cp_2Mg **gas flow rates of 5 and 10 sccm. (a) Sample D5; the diameter of NW is 76 nm and effective gate length is 2.3** μ**m. (b) Sample D10; the diameter of NW is 84 nm and effective length is 2.1** μ**m. Insets in (a) and (b) are** $I_{DS}-V_G$ **plots of the FETs at** V_{DS} **= 2 V.**

that metal electrodes with a higher work function should be more suitable for forming contact with p-type semiconductors. Therefore, we replaced the Ti/Au source–drain electrodes with Ni (100 nm)/Au (50 nm) electrodes to minimize the contact barrier. $I_{DS}-V_{DS}$ curves of a FET of D2 with Ni/Au electrodes became approximately linear (Figure 4b) as anticipated, further confirming the p-type conductivity of the doped NWs. Remarkably, the conductivity increased by more than 4 orders of magnitude to 0.11 Ω^{-1} cm^{-1} upon doping, which suggests that the Mg dopants can significantly tune the electrical transport properties of AlN NWs. Figure 4c shows the dependence of I_{DS} on V_G at V_{DS} = 2 V. On that basis, the hole mobility was deduced to be 1.13 cm^2/V s, increased by about 5 orders of magnitude compared to that of undoped NWs. The hole concentration (μ_h) is estimated to be about 6.1 × 10^{17} cm^{-3}. Furthermore, the log(I_{DS})$-V_G$ curve (Figure 3c) shows the on–off current ratio is greater than 10^4, indicating an obvious gate-control transport.

Similar FETs based on a single NW for samples D5 also display a p-type behavior, as depicted in Figure 5a. Significantly, the conductivity of sample D5 with an I_{DS} of ~10^{-6} A at V_{DS} = 2 V clearly shows a 10^6 times increase relative to that of the undoped sample; as a result the conductivity was further increased to ~8.4 Ω^{-1} cm^{-1}, which demonstrates that increasing the flow rate of the doping source can significantly enhance p-type conductivity in Mg-doped AlN NWs. Furthermore, the NW FETs cannot be turned off even at a gate voltage of −30 V. The transfer characteristics of sample D5 are shown in the inset in Figure 5a. Following the above calculation, the mobility of this Mg-doped AlN NW, sample D5, was derived to be about 6.4 cm^2/V s at V_{DS} = 2 V, and the hole concentration is estimated to be ~8.3 × 10^{18} cm^{-3}. Notably, the hole mobility for sample D5 in the present work is significantly larger than that of previously reported Mg-doped AlN films (~1 cm^2/V s)[2] and close to that of some similar types of 1D nanostructures such as p-type ZnO nanowires (10.5 cm^2/V s)[17] and Mg-doped GaN nanowires (12 cm^2/V s).[34] Furthermore, the present field-effect mobility also is comparable to that of Mg-doped GaN thin films (6–8 cm^2/V s) grown by molecular beam epitaxy technique.[35] It should be pointed out that although the hole mobility increased significantly, it was still much smaller than those observed in some III–V thin films with similar carrier concentration.[36,37] The low carrier mobility is considered to be due to the high surface-to-volume ratio of AlN NWs, which would enhance carrier scattering on the surface, leading to reduced carrier mobility as observed in Si NWs.[38] Furthermore, due to the employment of ammonia in the synthesis of Mg-doped AlN NWs, a large amount of H could be incorporated, which would deactivate the Mg acceptors and trap the free holes, as reported for Mg-doped AlN films grown by MOCVD.[2]

With a further increase of the dopant flow rate to 10 sccm (sample D10), the FETs show a weak gating effect; that is, $I_{DS}-V_{DS}$ curves are almost overlapping at different V_G (Figure 5b). However, for the same V_{DS}, the I_{DS} increases by about 7 orders of magnitude over that of the undoped AlN NWs, and the FET shows a high conductivity of 19.7 Ω^{-1} cm^{-1}. According to the $I_{DS}-V_G$ transfer curve at V_{DS} = 2 V (inset, Figure 5b), a similar analysis shows the FET has a hole mobility of ~2.5 cm^2/V s and a hole concentration of ~4.7 × 10^{19} cm^{-3}. This suggests that increasing the flow rate of the doping source to 10 sccm results in a higher carrier concentration.

According to the composition analyses, the effective hole concentration is much lower than the Mg concentration in the doped samples. This phenomenon has also been observed in heavily doped Si and ZnO nanowires.[32,39] According to previous reports,[25,40,41] the undoped AlN NWs should have intrinsic donor defects including Al$_i$, V$_N$, Si, and O impurities. When a small amount of Mg atoms are introduced into AlN crystals, some of them may first compensate the

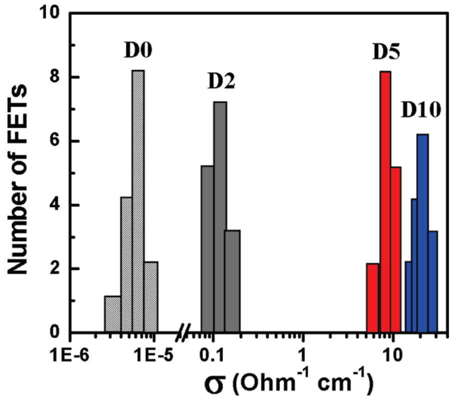

Figure 6. Distribution of conductivity for 60 FETs from undoped and Mg-doped AlN NWs. Fifteen FETs for each sample.

TABLE 1. Summary of Representative Carrier Concentration, Mobility, and Conductivity of Each Sample

	flow rate of Cp_2Mg (sccm)	carrier concentration (cm^{-3})	mobility (cm^2/V s)	conductivity (Ω^{-1} cm^{-1})
D0	0	1.7×10^{18}	2.3×10^{-5}	6.3×10^{-6}
D2	2	6.1×10^{17}	1.1	0.11
D5	5	8.3×10^{18}	6.4	8.4
D10	10	4.7×10^{19}	2.5	19.7

intrinsic donor defects.[28] In addition, some Mg dopants are not active due to the self-compensation effect, as observed in Mg-doped AlN films.[2] As a result, the effective carrier concentration is much lower than the Mg content in the doped samples.

Statistical Transport Properties of Mg-Doped AlN Nanowires. To assess the electrical properties with enough statistics, we have fabricated and measured at least 15 FETs based on a single NW from each sample. The transport measurements show good reproducibility. Figure 6 shows a statistical histogram of the conductivity. It can be seen that the conductivity of undoped AlN NWs is very low and in the range $(3.8-8.5) \times 10^{-6}$ Ω^{-1} cm^{-1}, whereas the conductivity drastically increases to $(0.9-1.6) \times 10^{-1}$ Ω^{-1} cm^{-1} for sample D2, to $6.1-10.6$ Ω^{-1} cm^{-1} for sample D5, and to $15.6-24.4$ Ω^{-1} cm^{-1} for sample D10. The above results clearly show that the p-type conductivity of AlN NWs can be tuned over a wide range of ~7 orders of magnitude by simply adjusting the flow rate of Mg doping gas during growth.

Table 1 summarizes the dependence of typical carrier concentration and mobility on the flow rate of Cp_2Mg vapor source. It is obvious that hole concentration increases continuously with increasing flow rate of Cp_2Mg gas and finally reaches 4.7×10^{19} cm^{-3} for sample D10, demonstrating that the carrier concentration in AlN NWs can be controlled by tuning the flow rate of the doping source. Nevertheless, the mobility first increases with increasing doping flow rate and then decreases at high flow rate. As observed in ZnO:Ga and CdSe:In nanowires,[32,42] the variation in hole mobility is considered to be due to improved semiconductor–metal contact for the Mg-doped NWs and to enhanced carrier scattering for the heavily doped samples. Note that the undoped sample has an extremely low mobility of about 2.3×10^{-5} cm^2/V s. Similar results have also been observed in some 1D nanostructures, such as CdSe,[42] ZnSe,[18] and ZnTe[43] nanowires. Significantly, the p-type conductivity in Mg-doped AlN NWs is highly reproducible and remains unchanged for more than three months.

CONCLUSIONS

In summary, we demonstrate the realization of p-type well-aligned AlN NW arrays with tunable electrical transport properties by Mg doping *via* a chemical vapor deposition process. The NWs are single crystalline and epitaxially grown on Si(111) substrates with [001] growth direction. Mg dopants distribute uniformly in AlN NWs with Mg content lower than 1.0 at. %. Field-effect transistors fabricated from a single NW for undoped and Mg-doped AlN NWs showed an obvious conversion from n-type conductivity in undoped NWs to p-type conductivity after Mg doping. By adjusting the doping gas (Cp_2Mg) flow rate from 0 to 10 sccm, the conductivity can be tuned over 7 orders of magnitude from $(3.8-8.5) \times 10^{-6}$ Ω^{-1} cm^{-1} for undoped sample to $15.6-24.4$ Ω^{-1} cm^{-1} for Mg-doped AlN NWs. The carrier concentration of p-type AlN NWs increases continuously with increasing flow rate of doping gas and approaches 4.7×10^{19} cm^{-3} at the heaviest doping. Significantly, the maximum hole mobility of ~6.4 $cm^2/(V$ s) is much larger that that of Mg-doped AlN films (~1 cm^2/V s),[2] and even comparable to that of Mg-doped GaN thin films (6–8 cm^2/V s).[35,39] This p-type behavior in Mg-doped AlN NWs is stable and remains unchanged for a period of over three months The capability of tuning p-type conduction and the understanding of the transport properties of AlN NWs will facilitate the development of AlN NW-based nanodevices such as deep-UV LEDs and photodetectors, as well as piezoelectric sensors.

EXPERIMENTAL SECTION

Undoped and Mg-doped AlN NWs were grown by a chemical vapor deposition method under similar growth conditions. A 2 g amount of $AlCl_3$ powder (99.9%, Aldrich) was placed in the sealed end of a small quartz tube, which was transferred to the center of the tube furnace, and Si(111) substrates were placed at the open end of the small quartz tube. During growth, the source and substrate temperatures were kept at about 400 and

750 °C, respectively. Bis(cyclopentadienyl)magnesium (Cp_2Mg) (99.9%, Aldrich) was evaporated at 180 °C by an independent heater (Figure S1) and subsequently transported by Ar to the reaction zone. Meanwhile, NH_3/Ar (1:4) was introduced into the furnace at a flow rate of 50 sccm. The flow rate of doping gas was tuned in the range 0−10 sccm to prepare nanowires with different doping concentrations. The reactions were carried out at atmospheric pressure, and the typical growth time was about 2 h. Undoped AlN NWs were prepared under the same conditions but with no dopant source.

The morphology of the as-synthesized AlN NW arrays was characterized by scanning electron microscopy. The crystal and microstructures and chemical components of the samples were analyzed using X-ray diffraction, transmission electron microscopy, high-resolution TEM, energy-dispersive X-ray spectroscopy, X-ray photoemission spectroscopy, and secondary ion mass spectroscopy.

For the fabrication of single NW FET, AlN NWs were collected from the Si substrate and dispersed in alcohol. The resulting NW suspension was then spread on a SiO_2 (300 nm)/p^+-Si wafer at a desired density. Patterned Ti (100 nm)/Au (50 nm) electrodes spaced 2 μm were then deposited on individual NWs by photolithography and electron-beam evaporation. Gate voltage was applied to the p^+-Si substrate in a standard global back-gate geometry. All FETs were annealed in N_2 at 500 °C for 10 min before electrical measurements.

Acknowledgment. The authors thank Dr. G. D. Yuan for his kind help in FET experiments. The work was supported by the IMR SYNL-T.S. Kê Research Fellowship, Research Grants Council of Hong Kong SAR, China (CityU101910).

Supporting Information Available: Schematic diagram of the apparatus for synthesizing the Mg-doped AlN NWs by a CVD method and typical XPS spectrum of Mg-doped AlN NW arrays. This information is available free of charge *via* the Internet at http://pubs.acs.org.

Note Added after ASAP Publication: After this paper was published online April 15, 2011, a correction was made to the Acknowledgment. The revised version was published April 20, 2011.

REFERENCES AND NOTES

1. Benjamin, M. C.; Wang, C.; Davis, R. F.; Nemanich, R. J. Observation of a Negative Electron-Affinity for Heteroepitaxial AlN on Alpha(6h)-SiC(0001). *Appl. Phys. Lett.* **1994,** *64*, 3288–3290.
2. Taniyasu, Y.; Kasu, M.; Makimoto, T. An Aluminium Nitride Light-Emitting Diode with a Wavelength of 210 Nanometres. *Nature* **2006,** *441*, 325–328.
3. Tondare, V. N.; Balasubramanian, C.; Shende, S. V.; Joag, D. S.; Godbole, V. P.; Bhoraskar, S. V.; Bhadbhade, M. Field Emission from Open Ended Aluminum Nitride Nanotubes. *Appl. Phys. Lett.* **2002,** *80*, 4813–4815.
4. Taniyasu, Y.; Kasu, M.; Makimoto, T. Field Emission Properties of Heavily Si-Doped AlN In Triode-Type Display Structure. *Appl. Phys. Lett.* **2004,** *84*, 2115–2117.
5. Liu, C.; Hu, Z.; Wu, Q.; Wang, X. Z.; Chen, Y.; Sang, H.; Zhu, J. M.; Deng, S. Z.; Xu, N. S. Vapor-Solid Growth and Characterization of Aluminum Nitride Nanocones. *J. Am. Chem. Soc.* **2005,** *127*, 1318–1322.
6. Zhao, Q.; Zhang, H.; Xu, X.; Wang, Z.; Xu, J.; Yu, D. P.; Li, G.; Su, F. Optical Properties of Highly Ordered AlN Nanowire Arrays Grown on Si Substrate. *Appl. Phys. Lett.* **2005,** *86*, 193101.
7. Yin, L. W.; Bando, Y.; Zhu, Y. C.; Li, M. S.; Li, Y. B.; Golberg, D. Growth and Field Emission of Hierarchical Single-Crystalline Wurtzite AlN Nanoarchitectures. *Adv. Mater.* **2005,** *17*, 110–114.
8. Shi, S. C.; Chen, C. F.; Chattopadhyay, S.; Chen, K. H.; Chen, L. C. Field Emission from Quasi-Aligned Aluminum Nitride Nanotips. *Appl. Phys. Lett.* **2005,** *87*, 073109.
9. Tang, Y. B.; Cong, H. T.; Zhao, Z. G.; Cheng, H. M. Field Emission from AlN Nanorod Array. *Appl. Phys. Lett.* **2005,** *86*, 153104.
10. He, J. H.; Yang, R.; Chueh, Y. L.; Chou, L. J.; Chen, L. J.; Wang, Z. L. Aligned AlN Nanorods with Multi-Tipped Surfaces: Growth, Field-Emission, and Cathodoluminescence Properties. *Adv. Mater.* **2006,** *18*, 650–654.
11. Song, X. B.; Guo, Z. G.; Zheng, J.; Li, X. G.; Pu, Y. K. AlN Nanorod and Nanoneedle Arrays Prepared by Chloride Assisted Chemical Vapor Deposition for Field Emission Applications. *Nanotechnology* **2008,** *19*, 115609.
12. Ji, X. H.; Zhang, Q. Y.; Lau, S. P.; Jiang, H. X.; Lin, J. Y. Temperature-Dependent Photoluminescence and Electron Field Emission Properties of AlN Nanotip Arrays. *Appl. Phys. Lett.* **2009,** *94*, 173106.
13. Harima, H.; Inoue, T.; Nakashima, S.; Okumura, H.; Ishida, Y.; Yoshida, S.; Koizumi, T.; Grille, H.; Bechstedt, F. Raman Studies on Phonon Modes in Cubic AlGaN Alloy. *Appl. Phys. Lett.* **1999,** *74*, 191–193.
14. Cheng, C. C.; Chen, Y. C.; Wang, H. J.; Chen, W. R. Low-Temperature Growth of Aluminum Nitride Thin Films on Silicon by Reactive Radio Frequency Magnetron Sputtering. *J. Vac. Sci. Technol. A* **1996,** *14*, 2238–2242.
15. Akiyama, M.; Morofuji, Y.; Kamohara, T.; Nishikubo, K.; Ooishi, Y.; Tsubai, M.; Fukuda, O.; Ueno, N. Preparation of Oriented Aluminum Nitride Thin Films on Polyimide Films and Piezoelectric Response with High Thermal Stability and Flexibility. *Adv. Funct. Mater.* **2007,** *17*, 458–462.
16. Kai, Y.; Yoshimura, M.; Mori, Y.; Sasaki, T. Synthesis of Low-Resistivity Aluminum Nitride Films Using Pulsed Laser Deposition. *Jpn. J. Appl. Phys.* **2003,** *42*, L229–L2331.
17. Yuan, G. D.; Zhang, W. J.; Jie, J. S.; Fan, X.; Zapien, J. A.; Leung, Y. H.; Luo, L. B.; Wang, P. F.; Lee, C. S.; Lee, S. T. P-Type ZnO Nanowire Arrays. *Nano Lett.* **2008,** *8*, 2591–2597.
18. Song, H. S.; Zhang, W. J.; Yuan, G. D.; He, Z. B.; Zhang, W. F.; Tang, Y. B.; Luo, L. B.; Lee, C. S.; Bello, I.; Lee, S. T. P-Type Conduction in Arsenic-Doped Znse Nanowires. *Appl. Phys. Lett.* **2009,** *95*, 033117.
19. Haber, J. A.; Gibbons, P. C.; Buhro, W. E. Morphological Control of Nanocrystalline Aluminum Nitride: Aluminum Chloride-Assisted Nanowhisker Growth. *J. Am. Chem. Soc.* **1997,** *119*, 5455–5456.
20. Yu., L. S.; Liu, N.; He, C. Y.; Wu, Q.; Hu, Z. *In-situ* Chloride-Generated Route to Different AlN Nanostructures on Si Substrate. *J. Phys. Chem. C* **2009,** *113*, 14245–14248.
21. Zhang, Y. J.; Liu, J.; He, R. R.; Zhang, Q.; Zhang, X. Z.; Zhu, J. Synthesis of Aluminum Nitride Nanowires from Carbon Nanotubes. *Chem. Mater.* **2001,** *13*, 3899–3905.
22. Yin, L. W.; Bando, Y.; Zhu, Y. C.; Li, M. S.; Tang, C. C.; Golberg, D. Single-Crystalline AlN Nanotubes with Carbon-Layer Coatings on the Outer and Inner Surfaces *via* a Multiwalled Carbon Nanotube Template Induced Route. *Adv. Mater.* **2005,** *17*, 213–217.
23. Wu, Q.; Hu, Z.; Wang, X.; Lu, Y.; Chen, X.; Xu, H.; Chen, Y. Synthesis and Characterization of Faceted Hexagonal Aluminum Nitride Nanotubes. *J. Am. Chem. Soc.* **2003,** *125*, 10176–10177.
24. Shi, S. C.; Chen, C. F.; Chattopadhyay, S.; Lan, Z. H.; Chen, K. H.; Chen, L. C. Growth of Single-Crystalline Wurtzite Aluminum Nitride Nanotips with a Self-Selective Apex Angle. *Adv. Funct. Mater.* **2005,** *15*, 781–786.
25. Zheng, J.; Yang, Y.; Yu, B.; Song, X. B.; Li, X. G. [0001] Oriented Aluminum Nitride One-Dimensional Nanostructures: Synthesis, Structure Evolution, and Electrical Properties. *ACS Nano* **2008,** *2*, 134–142.
26. Yang, Y.; Zhao, Q.; Zhang, X. Z.; Liu, Z. G.; Zou, X.; Shen, B.; Yu, D. P. Mn-Doped AlN Nanowires with Room Temperature Ferromagnetic Ordering. *Appl. Phys. Lett.* **2007,** *90*, 092118.
27. Tang, Y. B.; Cong, H. T.; Zhao, Z. G.; Cheng, H. M. Catalyst-Seeded Synthesis and Field Emission Properties of Flowerlike Si-Doped AlN Nanoneedle Array. *Appl. Phys. Lett.* **2006,** *89*, 253112.
28. Ji, X. H.; Lau, S. P.; Yu, S. F.; Yang, H. Y.; Herng, T. S.; Sedhain, A.; Lin, J. Y.; Jiang, H. X.; Teng, K. S.; Chen, J. S. Ultraviolet Photoluminescence from Ferromagnetic Fe-Doped AlN Nanorods. *Appl. Phys. Lett.* **2007,** *90*, 193118.

29. Ji, X. H.; Lau, S. P.; Yu, S. F.; Yang, H. Y.; Herng, T. S.; Chen, J. S. Ferromagnetic Cu-Doped AlN Nanorods. *Nanotechnology* **2007,** *18*, 105601.
30. Liu, Q. L.; Tanaka, T.; Hu, J. Q.; Xu, F. F.; Sekiguchi, T. Green Emission from c-Axis Oriented AlN Nanorods Doped with Tb. *Appl. Phys. Lett.* **2003,** *83*, 4939–4941.
31. Tang, Y. B.; Lee, C. S.; Chen, Z. H.; Yuan, G. D.; Kang, Z. H.; Luo, L. B.; Song, H. S.; Liu, Y.; He, Z. B.; Zhang, W. J.; *et al.* High-Quality Graphenes *via* a Facile Quenching Method for Field-Effect Transistors. *Nano Lett.* **2009,** *9*, 1374–1377.
32. Yuan, G. D.; Zhang, W. J.; Jie, J. S.; Fan, X.; Tang, J. X.; Shafiq, I.; Ye, Z. Z.; Lee, C. S.; Lee, S. T. Tunable N-Type Conductivity and Transport Properties of Ga-Doped ZnO Nanowire Arrays. *Adv. Mater.* **2008,** *20*, 168–173.
33. Nakamura, S.; Mukai, T.; Senoh, M.; Iwasa, N. Thermal Annealing Effects on P-Type Mg-Doped GaN Films. *Jpn. J. Appl. Phys.* **1992,** *31*, L139–L142.
34. Zhong, Z. H.; Qian, F.; Wang, D.; Lieber, C. M. Synthesis of P-Type Gallium Nitride Nanowires for Electronic and Photonic Nanodevices. *Nano Lett.* **2003,** *3*, 343–346.
35. Grandjean, N.; Massies, J.; Leroux, M.; Lorenzini, P. Ultraviolet GaN Light-Emitting Diodes Grown by Molecular Beam Epitaxy Using NH_3. *Appl. Phys. Lett.* **1998,** *72*, 82–84.
36. Lu, H.; Schaff, W. J.; Hwang, J.; Wu, H.; Koley, G.; Eastman, L. F. Effect of an AlN Buffer Layer on the Epitaxial Growth of InN by Molecular-Beam Epitaxy. *Appl. Phys. Lett.* **2001,** *79*, 1489–1491.
37. Wongchotiqul, K.; Chen, N.; Zhang, D. P.; Tang, X.; Spencer, M. G. In *Gallium Nitride and Related Materials*; Ponce, F. A., Dupuis, R. D., Nakamura, S., Edmond, J. A., Eds.; Material Research Society Symposium Proceedings, 1996; pp 279−282.
38. Jie, J. S.; Zhang, W. J.; Peng, K. Q.; Yuan, G. D.; Lee, C. S.; Lee, S. T. Surface-Dominated Transport Properties of Silicon Nanowires. *Adv. Funct. Mater.* **2008,** *18*, 3521–3527.
39. Cui, Y.; Duan, X.; Hu, J.; Lieber, C. M. Doping and Electrical Transport in Silicon Nanowires. *J. Phys. Chem. B* **2000,** *104*, 5213–5216.
40. Mattila, T.; Nieminen, R. M. *Ab Initio* Study of Oxygen Point Defects in GaAs, GaN, and AlN. *Phys. Rev. B* **1996,** *54*, 16676–166682.
41. Park, C. H.; Chadi, D. J. Stability of Deep Donor and Acceptor Centers in GaN, AlN, and BN. *Phys. Rev. B* **1997,** *55*, 12995–13001.
42. He, Z. B.; Jie, J. S.; Zhang, W. J.; Zhang, W. F.; Luo, L. B.; Fan, X.; Yuan, G. D.; Bello, I.; Lee, S. T. Tuning Electrical and Photoelectrical Properties of CdSe Nanowires *via* Indium Doping. *Small* **2009,** *5*, 345–350.
43. Cao, Y. L.; Tang, Y. B.; Liu, Y.; Liu, Z. T.; Luo, L. B.; He, Z. B.; Zhang, W. J.; Lee, C. S.; Lee, S. T. Coaxial Nanocables of P-Type Zinc Telluride Nanowires Sheathed with Silicon Oxide: Synthesis, Characterization and Properties. *Nanotechnology* **2009,** *20*, 455702.